Analysis of Distributed Energy Release Characteristics in an Ablative Pulsed Plasma Thruster

IEPC-2019-108

Presented at the 36th International Electric Propulsion Conference
University of Vienna • Vienna, Austria
September15-20, 2019

Lei Yang[1], Qi Liu[2], Xu Zhao[3]and Yuping Huang[4]
Beijing Research Institute of Precise Mechatronics and Controls, Beijing, 100076, China

Abstract: **Ablative pulsed plasma thruster (APPT) is one of the promising electric propulsion devices for micro-spacecraft missions. One of the main drawbacks of APPT is its inefficiency, for which several optimizations have been made to improve the thruster. Among these studies, the distributed release of energy stored in an APPT becomes a new strategy to improve performance. However, little research has been done on how to control the release of energy and the effects of propellant utilization and performance compared with regular APPT at the same energy level. In this paper, a rectangular double-discharge APPT（DD-APPT） prototype is built to further systematically analyze the distributed energy release characteristics and their impacts on discharge mechanism. The results show that the energy distribution conditions have a great influence on the discharge characteristics of DD-APPT. As the energy ratio of the primary and secondary capacitors decreases, there is a significant increase in efficiency and specific impulse at the same total energy (11.25J). Additionally, the time-of-flight (TOF) speed of fast ions entering the secondary discharge region is about 10-30km/s. Finally, emission spectroscopy tests indicate that the ionization degree of the ablated gas could be further promoted through a specific distributed energy release mode.**

Nomenclature

I_{bit}	=	impulse bit
m	=	mass
k	=	Boltzmann constant
I_{sp}	=	specific impulse
η	=	efficiency
L'	=	inductance gradient
I	=	discharge current
q	=	width
d	=	spectral lines shifts
α	=	ion broadening parameters
g	=	gravity acceleration
E	=	energy
t	=	time
λ	=	wavelength

[1]Senior Engineer, R&D center, ylforeverbit@126.com.
[2]Ph.D. candidate, R&D center, liuqi93922@163.com.
[3]Engineer, R&D center, 117380083@qq.com.
[4]Research Fellow, Institute Office, huangyp@2008.sina.com.

I. Introduction

Ablative Pulsed Plasma Thrusters (APPTs) are the first Electric Propulsion (EP) devices to fly onboard a real spacecraft (Zond-2) and until nowadays continue to be among the most reliable thrusters to be used as a part of the propulsion system of 50–150 kg spacecraft[1]. In its operations, short pulse discharges with several-microsecond duration are induced across an exposed propellant surface between electrodes, vaporizing and ionizing the surface. Then an interaction of the discharge current and its self-induced magnetic field results as Lorentz force acting on the plasma and inducing a directed plasma beam exhaust[2]. Since APPT has a repeatable and scalable impulse bit, it can be used for a wide range of missions from precise attitude control to orbit-maneuvers. In addition, the pulse characteristics of APPT allow it to be independent of continuous power supplies, and the high specific impulse per unit power (with the concomitant propellant savings) makes it an ideal candidate for increasing satellite payload to mass ratio[3].

Compared with other electric propulsion systems, the main disadvantage of an APPT is its relatively low efficiency. Conventional APPT has a typical thrust efficiency of 5–15% and a mean exhaust velocity lower than 10 km/s, whereas other plasma propulsion systems have the performance of 50% and 20–30 km/s[4]. Experimental studies have shown the low performance of APPT is caused by low propellant utilization[5]. The solid propellant (usually PTFE) continues to be ablated after the APPT discharge, due to the propellant temperature being above its sublimation point, which is known as late-time ablation (LTA). The late-time ablation creates a large number of neutral gas along the ablating surface, comprising of low-speed, and decomposed mixture of neutral atoms, monomers and free-radical chains of molecules ("slurry"). This neutral gas mostly account for most of ablated mass and has no contribution to the electromagnetic acceleration, which is the main reason for inefficiency of APPT.

To improve the thrust efficiency, researchers have performed several efforts to mitigate the production of LTA. These works pointed in several directions where improvement in performance can be obtained by keeping the propellant temperature down[6]. Although it is possible to reduce the LTA by operating at lower power, the LTA will still be produced. In recent years, research works focus on accelerating the LTA instead of trying to minimize it. The method had to be created to achieve such goals with the distributed release of energy stored in an APPT, hereby called high frequency burst or dual-stage [7-8]. The essence of this method is to utilize the effects of the LTA on the performance by employing additional discharges after the main discharge. Therefore, some researchers have allocated APPT energy to two or more capacitors and then release them to provide additional discharge[9]. Nevertheless, the improvements in previous studies were not analyzed and compared with conventional APPT in detail at the same energy level. Furthermore, some researchers designed a double-discharge APPT（DD-APPT） and evaluated the effect of energy distribution at the same total energy[10]. However, the duration of the secondary discharge under these conditions were only slightly greater than or equal to the counterpart of the main discharge, which cannot effectively ionize and accelerate the late-time ablated gas.

In our study, a rectangular DD-APPT prototype is built to further systematically analyze the distributed energy release characteristics and its impact on discharge mechanism. The total energy is allocated to two capacitors, which discharge separately in two sets of isolated electrodes. And the second discharge cycle is designed to be long enough to ionize and accelerate the LTA gas as much as possible. Discharge tests under the six different distribution conditions at the same total energy (11.25J) are carried out. Then, the performance of the DD-APPT was evaluated by experimental data and compared and analyzed with conventional APPT. Finally, the effect of ionization and acceleration of LTA gas in DD-APPT working process is discussed.

II. Experimental apparatus

The experimental system included three sections: the vacuum system and the DD-APPT prototype, and the measurement system.

A. Vacuum system and DD-APPT prototype

All of the experiments are taken in a stainless steel vacuum chamber with 1m in diameter, and 0.65m in length that is pumped down by a two-stage vacuum pump system to an operating pressure of about 5×10^{-3}Pa prior to experiment.

The rectangular DD-APPT prototype used in this experiment has a parallel electrode configuration which uses PTFE as propellant, which is shown in Fig.1. A breech-fed configuration of the PTFE propellant is spring fed to the electrodes. The first two electrodes (cathode 1 and anode 1) are placed in contact with the propellant surface and are mainly responsible for the ablation process. In order to initiate the discharge, a spark plug is located in the cathode 1. The second two electrodes(cathode 2 and anode 2) are placed downstream to avoid generating more late-time ablation. The width and thickness of the electrode are 18 and 10 mm, respectively, and the spacing is 52 mm. The length of insulated channel is 25mm. The DD-APPT prototype has a 10μF capacitor for the primary discharge and a 295μF capacitor for the secondary discharge. The purpose of selecting a high capacitance of the secondary discharge is to increase the duration of secondary discharge to effectively utilize LTA gas. The power supply for the DD-APPT prototype mainly includes the adjustable primary discharge circuit and secondary discharge circuit, the 500 V trigger circuit and the trigger control circuit. The power supply accepts a commonly used AC 220V 50 Hz voltage and converts it to a 0-2 kV adjustable DC for primary discharge and secondary discharge, and 500 V DC needed by the spark plug. The operating principle of DD-APPT prototype is simple: spark plug ignition provides the initial charged particles to trigger the primary discharge to generate plasma. A secondary discharge is triggered when the plasma moves to the second two electrodes(cathode 2 and anode 2). Then the LTA gas will serve as the propellant for the secondary discharge and also be accelerated that will take place downstream.

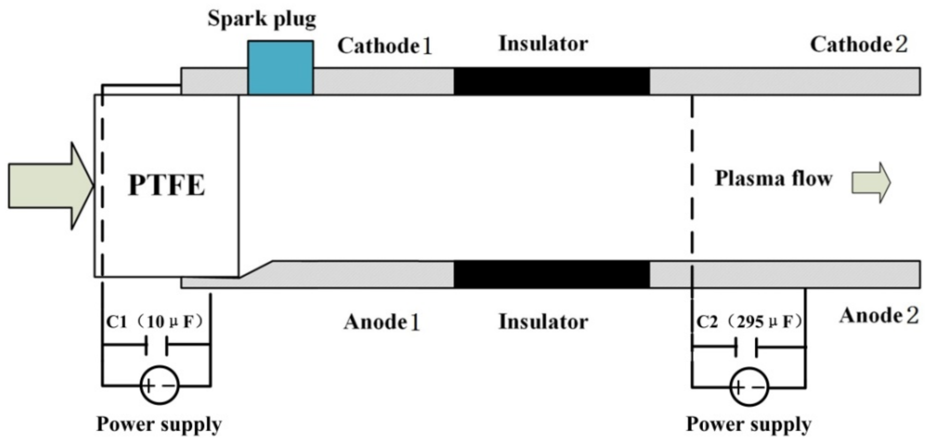

Figure 1. Schematics of the experimental DD-APPT.

B. Measurement system

Two Agilent 10076C high voltage probes (parameters are shown in Table 1) are used to test the primary discharge voltage and the secondary discharge voltage, respectively. The current sensors (parameters are shown in Table 2) including Rogowski coil and the follow-up external integrator circuit are used to measure the instantaneous pulsed high-current of the primary discharge and the secondary discharge. The outer ring is PTFE core holder, winding a 4×0.27 mm-diam copper wire on a 2-mm-diam polymer rod. The wire is wrapped in 400 turns in two layers. The outer layer uses epoxy resin seal to achieve insulation and anti-hypertension. The ends of the Rogowski coil are connected to an RC integration circuit to obtain a linear relationship between the measured value and the discharge current. Rogowski coils are placed in the discharge circuit of the primary and secondary electrodes in the vacuum chamber, and the signals are output to the oscilloscope through the integrating circuit outside the chamber.

Table 1.Parameters of voltage probes

Parameters	Value
Bandwidth (-3dB)	500Mhz
Rising time	＜0.7ns
Decay ratio	100:1
Maximum input	4000V peak

Table 2.Parameters of current sensors

Parameters	Value
Sensitivity	4.7×10^{-4} V/A
Integration circuit time constant	54 μs
Maximum input	50kA
Coil withstand voltage	＜1kV

Further optical emission spectroscopy (OES) methods are used to investigate plasma characteristics in the double-discharge. For the experiments in this study, the spectral lines are obtained by a Sofn 7ISW303 spectrometer (parameters are shown in Table 3) with 10 μm~3mm entrance slit width and with 14 μm entrance slit height. The spectrometer has three standard optical grating (wavelength range of 330-828nm) and grating size is 55nm×55nm. A collimation system with two lenses collects the light signal of end-on view which is perpendicular to the fiber. Fixed position is calibrated by detecting a probe light laser. In addition, the Sartorius CPA225D high-precision electronic balance is used to measure the DD-APPT ablated mass. The balance has an accuracy of 0.1 mg for weighing objects below 220 g, and an accuracy of 0.01 mg for weighing objects of 100 g or less. The mass of consumed propellant are collected as averages over the DD-APPT's 1000 shots.

Table 3.Parameters of spectrometer

Parameters	Value
Focal length	300nm
Stray light	5×10^{-4}
Minimum step	0.0023nm
Grating size	55nm×55nm
Standard grating	70G1200-300(1200g/mm, λ_p=300nm) 70G600-750(600g/mm, λ_p=750nm) 70G300-1250(300g/mm, λ_p=1250nm)

The schematic diagram of the measurement system is shown in Fig. 2.

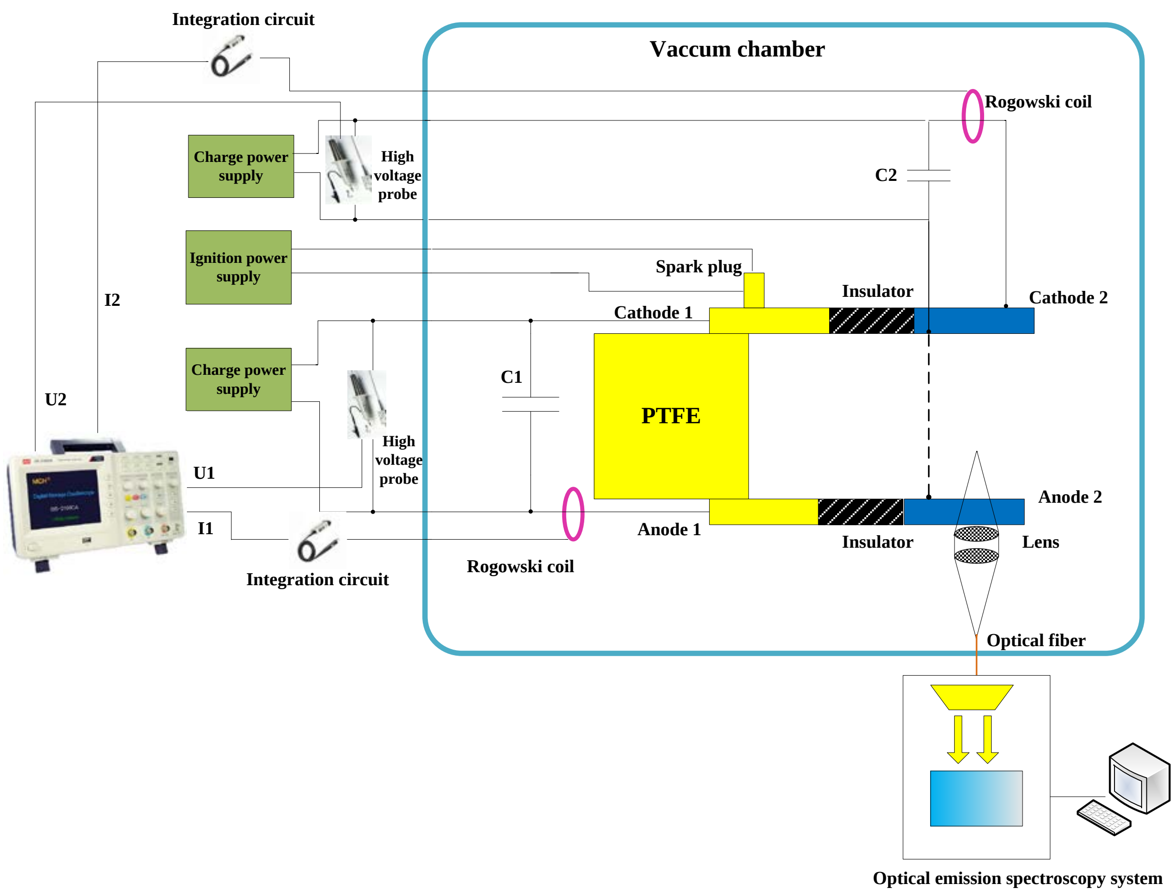

Figure 2. Schematic diagram of the measurement system.

III. Results and discussion

A. Discharge mechanism

Preliminary tests under six working conditions at the same total energy (11.25J) are carried out. The initial volta ges corresponding to the different working conditions are shown in Table 4.

Table 4.Initial voltages of primary and secondary capacitors for the six different working conditions

Number	Primary voltage, V	Secondary voltage, V	Energy distribution
1	1500	0	N/A
2	1400	100	6.64:1
3	1300	138	3:1
4	1200	166	1.77:1
5	1100	188	1.16:1
6	1000	206	0.8:1

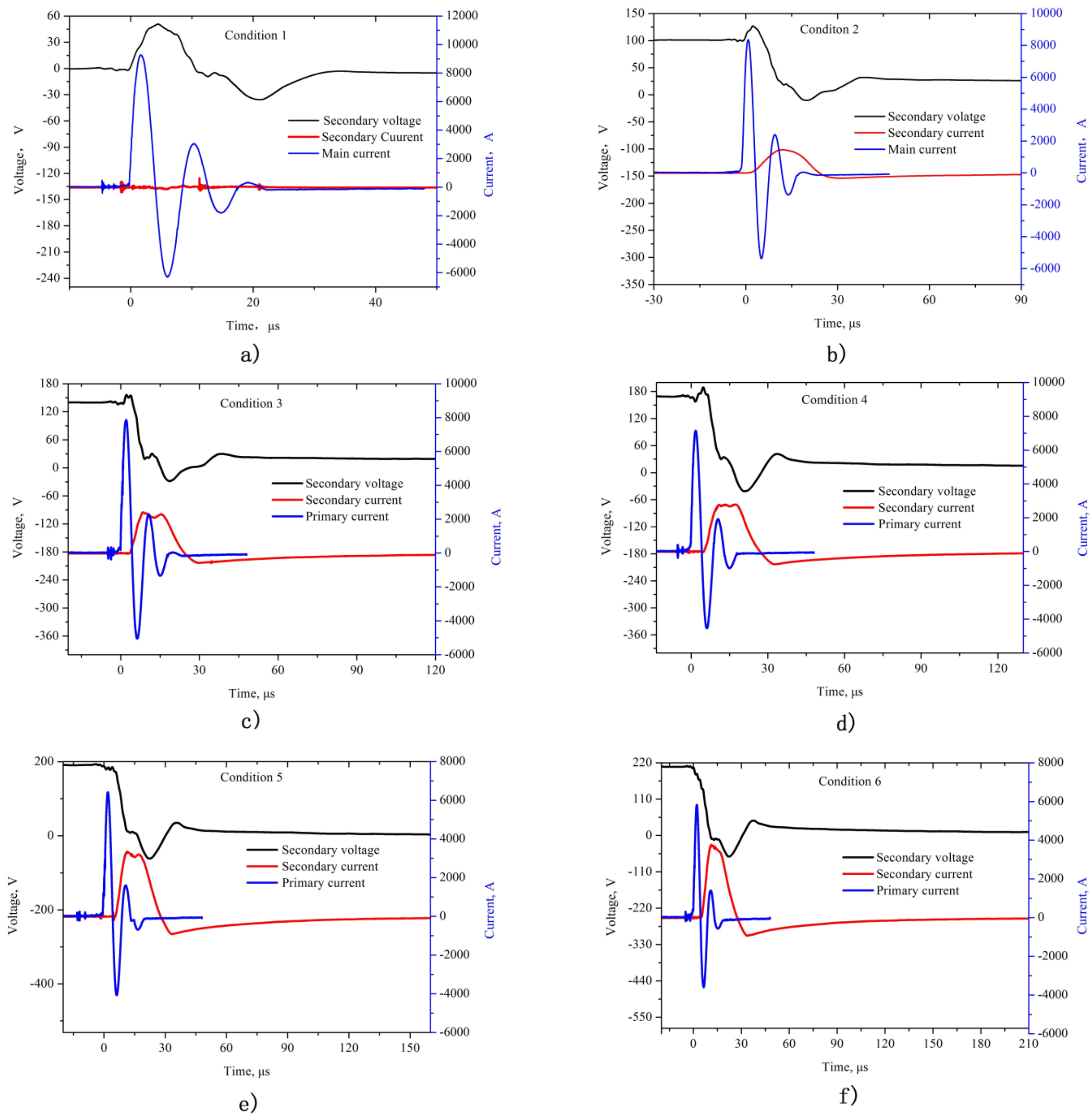

Figure 2. Voltage and current waveforms under different working conditions.

The results show that the energy distribution conditions have a great influence on the discharge characteristics of DD-APPT, as shown in Fig. 2. The current waveform of the primary capacitor is basically the same as the regular PPT. The secondary capacitor has a very obvious working process of charging first and then discharging again. This process is produced by the plasma generated by the discharge of the main electrodes reaching the secondary electrodes. The voltage of the secondary capacitor gradually rises due to the charging. When the voltage is high enough to cause breakdown between the secondary electrodes, a discharge phase occurs, and the stored electrical energy is released in a period of several tens or even hundreds of microseconds, and the secondary discharge operation mode is completed. The charging effect of the second capacitor reduces as the energy ratio of the primary and secondary capacitors decreases. When the energy ratio is below 1.2 (i.e., conditions 5 and 6), the secondary capacitor only operates in the discharge mode. In contrast, the secondary discharge duration increases as the energy ratio decreases. Condition 6 has a discharge time of more than 200μs, which is much larger than the primary discharge duration. This means that the secondary discharge would be flowing on the late-time ablated gas under such conditions. Therefore, under the condition that the total energy storage of DD-APPT is constant, appropriately increasing the initial energy of the secondary capacitor is instrumental to accelerate the LTA gas.

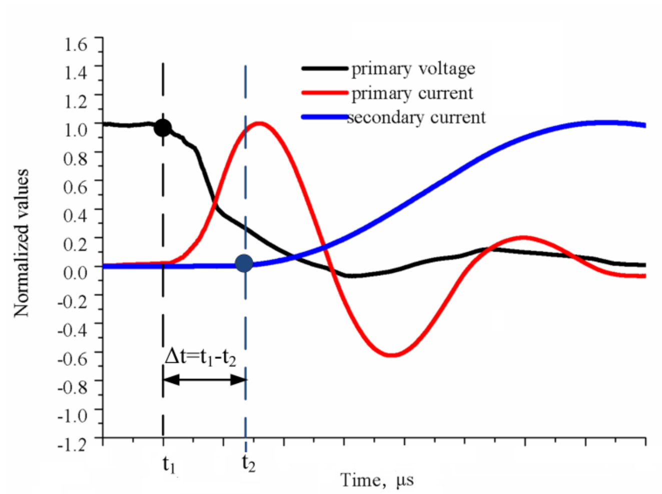

Figure 3. The time difference between primary discharge initiation and the onset of a recorded secondary current signal used for time-of-fight measurements.

Based on the voltage and current signals of the DD-APPT, we can get the time difference Δt between the two discharges as shown in Fig. 3. Thus, we can calculate the time-of-flight (TOF) velocity of plasma coming out from the first stage and reaching the second electrode set.

$$V_{TOF} = \frac{\Delta x}{\Delta t} \quad (1)$$

where Δx is the length of the insulated channel between the two pairs of electrodes.

Simple TOF measurements indicated that the velocity of fast charged particles entering the secondary discharge region is about 10-30km/s and the TOF value rises linearly as the primary discharge energy increases, as shown in Fig. 4.

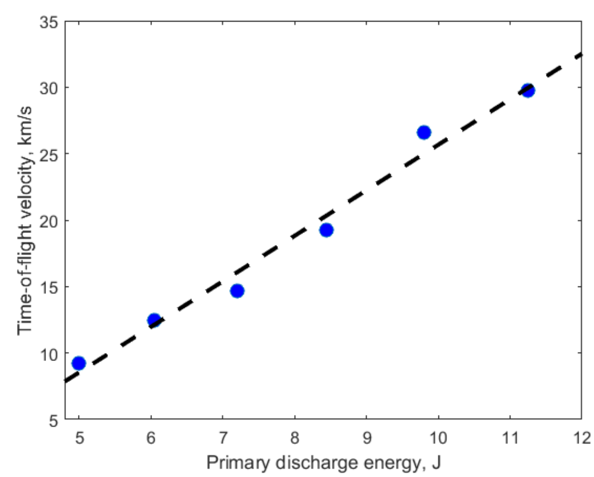

Figure 4. Time-of-flight velocity of the plasma coming out from the first stage and reaching the secondary electrode set as a function of primary discharge energy.

B. Performance evaluation

Knowing the discharge current curves of an APPT allows for the inference of the electromagnetic impulse bit I_{EM}. The estimation of the I_{EM} can be obtained with the following equation[11]

$$I_{EM} = \frac{1}{2} L' \int_0^t \left[I(t) \right]^2 d\tau \quad (2)$$

where I is the instantaneous discharge current and L' is the inductance gradient of the electrodes.

The inductance gradient L' depends on the electrode size, which can be easily calculated by[12]

$$L'(\mu H/m) = \frac{dL}{dl} = 0.4 \ln \frac{h}{w+c} + 0.6 \quad (3)$$

where h, w and c are the spacing, width and thickness of the electrodes, respectively.

The electromagnetic term is used because in this calculation we do not take the impulse produced by non-ionized propellant into account. This calculation method is useful when a thrust balance is not available and can give an insight of the performance parameters. Therefore, the total impulse bit of a DD-APPT can be approximated by the sum of the electromagnetic impulse bit of the two discharges[9]:

$$I_{bit} = I_{EM1} + I_{EM2} = \frac{1}{2} L_1' \int_0^{t_1} \left[I_1(t) \right]^2 d\tau + \frac{1}{2} L_2' \int_{t_s}^{t_2} \left[I_2(t) \right]^2 d\tau \quad (4)$$

where $L_1^{'}$ and $L_2^{'}$ are the inductance gradients of the two sets of electrodes, t_s is the time at which the secondary discharge starts, and t_1 and t_2 are the times at which the primary and secondary discharges end, respectively. I_1 is the currents of the primary discharge and I_2 is the currents of the secondary discharge.

In order to calculate the specific impulse of a DD-APPT we need the ablated mass Δm, which is the propellant consumed in a discharge. This is obtained by weighting the propellant before and after many shots and then averaging the value for a discharge. The average electromagnetic specific impulse I_{sp} can then be calculated:

$$I_{sp} = \frac{I_{bit}}{\Delta m \cdot g} \quad (5)$$

The electromagnetic total efficiency is calculated as

$$\eta = \frac{I_{bit}^2}{2\Delta m \cdot E_0} \quad (6)$$

where E_0 is the total energy stored in the capacitors of a DD-APPT. In the experimental conditions of this paper, E_0 is 11.25J.

A sample of the performance calculations of the DD-APPT prototype under working conditions 1 and 4 in Table 4 are shown in Table 5.

Table 5. A sample of the performance calculations under test conditions 1 and 4

Working conditions	Total impulse bit, μNs	specific impulse, s	Efficiency, %	Ablated mass, μg
1	124	931	5.1	13.3
4	112	1304	6.5	8.6

Performance calculations show that the specific impulse and efficiency of Condition 4 are about 40% and 1.4% higher than Condition 1(regular APPT working condition) at the same energy, respectively. The specific impulse increases as the energy in the secondary discharge increases. This is understandable as the energy on the secondary discharge is used to further accelerate the plasma and LTA gas coming out from the first stage. Since the secondary discharge takes place relatively far from the propellant surface and will not produce LTA, the total ablated mass is directly and linearly proportional to the primary discharge energy. This means that when the total energy of DD-APPT is constant, the increase in the proportion of secondary discharge energy will result in a decrease in the total ablated mass. This behavior has correlation with results of ablated mass presented in Table 5. When DD-APPT is working at condition 4, the ablated mass is reduced by 35% compared to condition 1. It can be seen from Eq.5 and Eq.6 that the ablated mass directly affects the specific impulse and efficiency. Therefore, although the DD-APPT has a slight decrease in the total impulse bit at the condition 4, the specific impulse and the efficiency are greatly improved due to the reduction in the ablated mass.

C. Plasma characteristics

In the experiment, emissions around CII wavelengths with high intensity are measured and selected as representations of PPT plasma. Under the assumption of LTE and the energy level population distributed according to the Boltzmann law, the relative intensity is given by[13]

$$\ln\left(\frac{\varepsilon_{mn}\lambda_{mn}}{g_m A_{mn}}\right) = \ln\frac{N}{Z} - \frac{E_m}{kT} \quad (7)$$

where ε_{mn} is the relative intensity, A_{mn} is the transition probability from the upper state m to the lower stare n, λ_{mn} is the wavelength of CII, g_m is the statistical weight of upper state, N is the total number density, and Z is the partition function.

Therefore, electron temperature can be derived from the slope of the Boltzmann plot, without knowing the values of n and Z. A sample plot of the left-hand-side of Eq. 7 using the experimentally acquired lines (i.e., 391.898nm, 588.977nm or 658.288nm) in the primary discharge exit area (Condition 1) is shown in Fig.5, where each of the points represents data (peak voltage of spectral line intensity) averaged over ten shots. A least squares linear fit is also illustrated. The linear fit indicates that the peak electron temperature is about 12500K, which agrees quite well with other works[14].

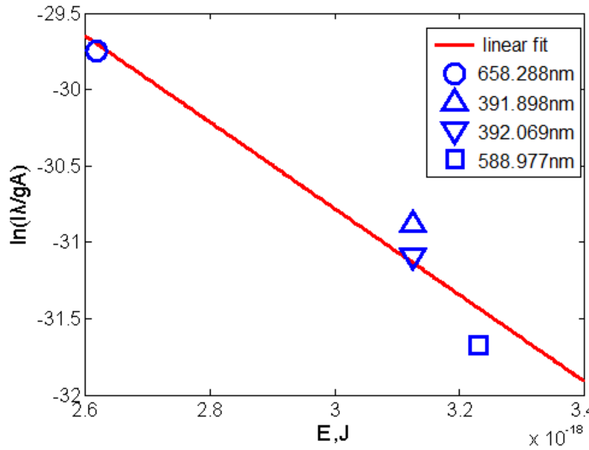

Figure 5. Fitted Boltzmann curve.

Profiles of the spectral lines emitted from plasma are subject to various broadening and shifting mechanisms such as Doppler broadening, resonance, van der Waals and Stark broadening. Van der Waals and resonance broadening are small enough to be neglected and Doppler broadening is calculated in the order of 10^{-3}nm which is much smaller than Stark broadening. Thus electron density was determined by Stark FWHM of C II 658nm spectral line for our experimental conditions:

$$\Delta\lambda_s = \left[(d/q) + 2.0\times10^{-4} N^{1/4} \alpha \left(1 - 0.068 N^{1/6} T^{-1/2}\right)\right] 10^{-16} qN \quad (8)$$

where the parameters q, d and α are taken from literature and interpolated for the given temperature[15].

A sample of six wavelengths of CII near 658nm are used to fit Lorentzian Profile shown in Fig.6. The test results of DD-APPT working under condition 1 indicate that the plasma is concentrated mainly near the propellant during PPT discharge. As the plasma moves downstream, the values of electron density decrease, and the peak electron density at the secondary discharge inlet region is approximately 5×10^{16}cm^{-3}. DD-APPT working at condition 1 can be considered a regular APPT. In order to analyze the ionization effect of the secondary discharge on the plasma generated by the main discharge and the subsequent incoming LTA gas, the electron density of DD-APPT operating at condition 6 is further tested. The results show that the peak electron density at the secondary discharge inlet region under condition 6 is 2×10^{17}cm^{-3}, which is larger than condition 1by an order of magnitude. This indicates that the APPT can further increase the ionization degree of the ablated gas through a specific distributed energy release mode.

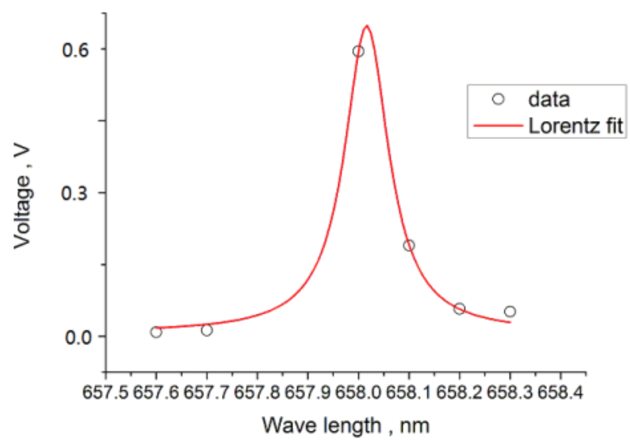

Figure 6. Lorentz fitting with the data of six wavelengths of CII near 658nm.

IV. Conclusion

The distributed energy release characteristics and its impact on discharge mechanism of a rectangular DD-APPT prototype have been tested and analyzed under different working conditions at the same total energy. The secondary capacitor has a very obvious working process of charging at first and then discharging again. To overcome this first charging process and only initiate the positive only discharge mode it is necessary to appropriately increase the secondary discharge energy of DD-APPT under the same energy and satisfying the initial discharge of the primary capacitor. The present data suggests that long-period secondary discharge can effectively accelerate LTA gas, thereby increasing the specific impulse and efficiency of DD-APPT. However, further experiments will be needed to deeply understand and develop this new scheme both experimentally and theoretically. Finally, emission spectroscopy measurements reveal plasma characteristics of DD-APPT under different operating conditions. This study provides a physical mechanism for double-discharge pulsed plasma thrusters.

Future work include direct measurements of the impulse of the DD-PPT in order to take into account the thrust produced by the gas-dynamic contribution and also to confirm calculated performance data based on current measurements.

Acknowledgments

This work was supported by National Natural Science Foundation of China (Grant No. 11602016).

References

[1] Antipov A. A., Bogatyy A. V., and Semenov A. A., "Investigation of the Initial Stage of the Discharge in an Ablative Pulsed Plasma Thruster," *Journal of Surface Investigation: X-ray, Synchrotron and Neutron Techniques*,, Vol. 12, No. 5, 2018, pp. 1037-1040.

[2] Burton, R. L., and Turchi, P. J., "Pulsed Plasma Thruster," *Journal of Propulsion and Power*, Vol. 14, No. 5, 1998, pp. 716-735.

[3] Popov G.A., and Antropov N.N., "Ablative PPT. New quality, new perspectives,," *Acta Astronautica*, Vol. 59, 2006, pp. 175-180.

[4] Koizumi, H., Noji, R., Komurasaki, K., and Arakawa, Y., "Plasma acceleration processes in an ablative pulsed plasma thruster," *Physics of Plasmas*, Vol. 14, 2007, pp. 033506.

[5] Schönherr, T., Komurasaki, K., and Herdrich, G., " Propellant Utilization Efficiency in a Pulsed Plasma Thruster," *Journal of Propulsion and Power*, Vol. 29, No. 6, 2013, pp. 1478-1487.

[6] Antonsen E. L., Burton, R. L., Reed G. A., and Spanjers G. G., " Effects of Postpulse Surface Temperature on Micropulsed Pulsed Plasma Thruster," *Journal of Propulsion and Power*, Vol. 21, No. 5, 2005, pp. 877-882.

[7] Marques R. I., Gabriel, S. B., and Costa F. de S., " High Frequency Burst Pulsed Plasma Thruster Research at the University of Southampton," *30th International Electric Propulsion Conference,* IEPC-2007-300, Florence, Italy, 2007.

[8] Li, Y. H., and Royer, C., "Effect of voltage on second-stage electrodes of dual-stage solid propellant pulsed plasma thruster," *Vacuum*, Vol. 167, 2019, pp. 103-112.

[9] Marques R. I., Gabriel, S. B., and Costa F. de S., "The Two-Stage Pulsed Plasma Thruster," *31st International Electric Propulsion Conference,* IEPC-2009-250, Ann Arbor, Michigan, USA, 2009.

[10] Wu, Z., Sun, G., Huang, T., Liu, X., Xie, K., and Wang, N., "Optimization of the Energy Distribution in Ablative Pulsed Plasma Thrusters," *Journal of Propulsion and Power*, Vol. 56, No. 8, 2018, pp. 3024-3033.

[11] Jahn, R. G., *Physics of Electric Propulsion*, McGraw-Hill, New York, 1968.

[12] Burton R L., Wilson M J., and Bushman S S., "Energy Balance and Efficiency of the Pulsed Plasma Thruster," *34th AIAA/ASME/SAE/ASEE Joint Propulsion Conference and Exhibit,* AIAA-1998-3808, Cleveland, OH , USA, 1998.

[13] Markusic, T. E., and Spores, R. A., "Spectroscopic emission measurements of a pulsed plasma thruster plume," *33rd AIAA/ASME/SAE/ASEE Joint Propulsion Conference,* AIAA-1997-2924, Seattle, WA , USA, 1997.

[14] Schönherr, T., Nees, F., Arakawa, Y., Komurasaki, K., and Herdrich, G., "Characteristics of Plasma Properties in an Ablative Pulsed Plasma Thruster," *Physics of Plasmas*, Vol. 20, 2013, pp. 033503.

[15] Griem, H. R., *Plasma Spectroscopy*, McGraw-Hill, New York, 1964.